Quantum-size-induced electronic transitions in quantum dots: Indirect band-gap GaAs

Jun-Wei Luo, Alberto Franceschetti, and Alex Zunger*
National Renewable Energy Laboratory, Golden, Colorado 80401, USA
(Received 27 December 2007; published 7 July 2008)

We discuss the physical origin of the previously predicted quantum-size-induced electronic transitions in spherical GaAs quantum dots. By using atomistic pseudopotential calculations for freestanding GaAs dots and for GaAs dots embedded in an AlGaAs matrix, we are able to distinguish two types of direct/indirect transitions: (i) in freestanding GaAs dots, the conduction-band minimum changes from Γ-like to X-like as the radius of the dot is reduced below 1.6 nm, leading to a direct/indirect transition in reciprocal space. (ii) In GaAs dots embedded in AlAs, the conduction-band minimum changes from dot localized to barrier localized as the radius of the dot is reduced below 4.2 nm, corresponding to a direct-to-indirect transition in real space.

DOI: 10.1103/PhysRevB.78.035306 PACS number(s): 73.21.La, 73.22.−f, 64.70.Nd

I. INTRODUCTION

Semiconductor nanostructures are often advertised[1,2] as having the potential for stronger light absorption than the bulk materials from which they are made. This property of quantum dots makes them ideal candidates for optoelectronic applications such as tunable lasers,[3,4] light-emitting diodes,[5] and biological markers.[6] For such applications, it is highly desirable for the band-edge optical transitions to be direct, both in real space and in reciprocal space. A transition is "direct in real space" if the wave functions of the initial and final states are located in the same real-space domain, e.g., in the interior of the quantum dot. A transition is "direct in reciprocal space" if the initial and final wave functions originate from the same region of the Brillouin zone of the bulk material from which the quantum dot is made. It was previously predicted[7–10] that a nanostructure made of a direct-gap semiconductor material, such as GaAs, does not necessarily have direct band-edge optical transitions because quantum-confinement effects can lead to changes in the order of the energy levels, altering the band gap from direct to indirect either in real space or in reciprocal space. We distinguish and explain here two such types of electronic transitions:

Type-(i): Direct-to-indirect transition in reciprocal space [Fig. 1(a)]. This type of electronic transition describes for example the transformation of the conduction-band minimum (CBM) of a semiconductor nanostructure from Γ-like to X-like upon quantum confinement, while the valence-band maximum (VBM) remains Γ-like at all sizes. Type-(i) transitions can occur if the CBM of the bulk material has a smaller effective mass than higher-energy conduction-band valleys, and the energy difference between these states in the bulk is small enough to be overcome by differential quantum confinement.[7,8] This type of electronic transition was predicted to occur in freestanding GaAs nanocrystals.[7,8]

Type-(ii): Direct-to-indirect transition in real space [Fig. 1(b)]. This type of electronic transition involves an upward shift of the CBM of the quantum dot above the CBM of the barrier, thereby making the band gap indirect in real space.[7,10] If the CBM of the barrier originates from a different conduction-band valley in the Brillouin zone, the direct/indirect transition in real space will simultaneously occur with a direct/indirect transition in reciprocal space. This type of electronic transition was predicted to occur in GaAs dots embedded in AlGaAs.[7,10]

Type-(i) electronic transitions in GaAs freestanding nanostructures have been studied before.[8–11] In Ref. 9, we used atomistic pseudopotential calculations to study the direct/indirect transition in two-dimensional GaAs *films* and one-dimensional GaAs *wires*. We also found that the band gap of small, parallelepipedal GaAs *dots* is *indirect* in reciprocal space, with the VBM originating from the bulk Γ_{15v} states and the CBM originating from the bulk X_{1c} states. However, due to computer limitations a decade ago, we were not able

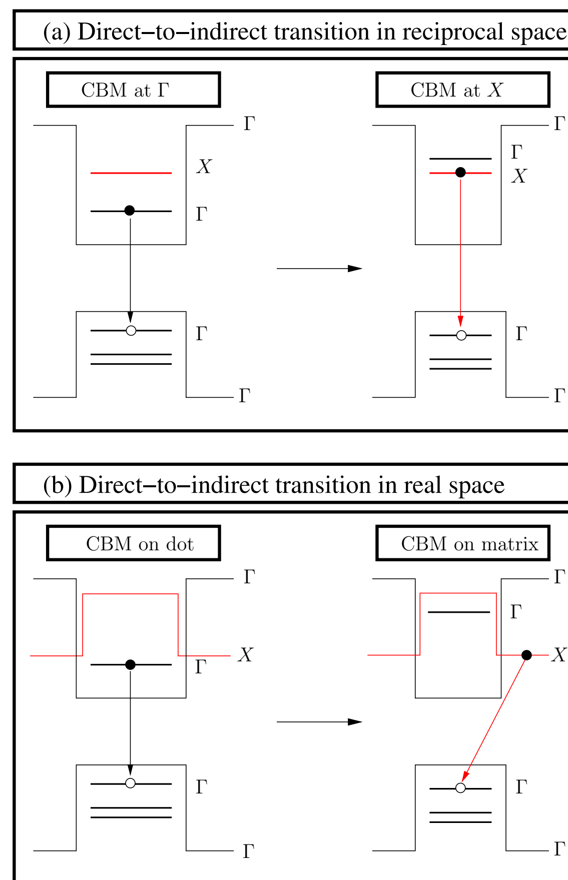

FIG. 1. (Color online) Schematic of two types of direct-to-indirect transitions in semiconductor quantum dots.

 ©2008 The American Physical Society

to observe the direct/indirect transition in GaAs dots. Díaz and Bryant[8] recently reported nearest-neighbor tight-binding calculations of spherical GaAs nanocrystals ranging in radius from 1 to 7 nm. They found that for dot sizes below 1.25 nm in radius, the band gap is indirect in reciprocal space, with the CBM primarily originating from the *L -point bulk states*. Thus, there is an apparent contradiction between tight-binding calculations[8] that predicted a Γ-to-*L* transition at small dot sizes, and pseudopotential calculations[9] that predicted an *X*-like CBM in small GaAs quantum dots. The description of type-(i) electronic transitions in nanostructures requires not only an accurate depiction of the effective-mass tensors of the relevant states (Γ_{1c}, X_{1c}, and L_{1c}), but also an accurate representation of the wave functions, because different wave functions may couple near the transition point. We find here via accurate pseudopotential calculations that in spherical GaAs quantum dots, the type-(i) transition occurs between Γ and *X* (in agreement with Ref. 9). Specifically, the CBM of freestanding GaAs quantum dots becomes *X*-like for quantum-dot radii smaller than 1.65 nm. This transition is not accurately described by the single-band effective-mass approximation, in which the type of crossing (Γ-*X* or Γ-*L*) depends on the choice of how the different components of the anisotropic *X* and *L* effective masses are assembled into a single value.

Type-(ii) electronic transitions in GaAs quantum dots embedded in an $Al_xGa_{1-x}As$ alloy were studied in Ref. 10 by using the single-band effective-mass approximation (EMA). It was found that the CBM of this system undergoes a real-space (type ii) electronic transition when the radius of the GaAs quantum dot drops below a critical value $R_c(x)$, which depends on the Al concentration x of the alloy. For $x>0.4$, the CBM of the $Al_xGa_{1-x}As$ alloy originates from the *X* point, so the real-space (type ii) transition simultaneously occurs with a reciprocal-space (type i) transition. Empirical pseudopotential calculations have later shown[11] that this transition is characterized by a Γ-*X* *anticrossing*, with an anticrossing splitting of ~2 meV.

II. METHOD

The single-particle electronic states of a quantum dot are described here by using the empirical pseudopotential method (EPM).[12] The crystal potential is given by the superposition of screened atomic potentials v_α (for atom type α) located at positions $\mathbf{R}_{\alpha,n}$: $V(\mathbf{r})=\Sigma_{\alpha,n}v_\alpha(\mathbf{r}-\mathbf{R}_{\alpha,n})$. The pseudopotentials v_α are fitted to experimental transition energies, effective masses, and deformation potentials of the bulk constituents. The EPM energy levels and effective masses are compared to the experimental results[13] in Table I, where we also give first-principles[14,15] and tight-binding[16] results. To investigate the type-(i) transition, we consider freestanding GaAs nanocrystals up to $Ga_{1436}As_{1433}$ [radius $R=2.49$ nm (Ref. 17)]. The GaAs dots are embedded in a wide-gap artificial barrier in order to obtain large conduction-band and valence-band offsets. To investigate the type-(ii) transition, we consider GaAs spherical quantum dots embedded in AlGaAs. The supercell contains up to a total of 110,592 atoms. The Schrödinger equation is solved by expanding the wave functions $\psi_i(\mathbf{r})$ in a plane-wave basis set for small systems,[18] or in a linear combination of Bloch bands (LCBB) for large systems.[19]

TABLE I. Γ, *X*, and *L* energies and effective masses of bulk GaAs from the present empirical pseudopotential description and from LDA[14,15] and tight-binding (TB).[16] Here, Δ(Γ-*L*) and Δ(Γ-*X*) denote the Γ-to-*L* and Γ-to-*X* conduction-band spacings, respectively. Experimental results at low temperature are taken from Ref. 13.

Properties	LDA[a]	TB[b]	Present EPM	Expt.[c]
$E(\Gamma_{1c})$	0.16	1.41	1.52	1.52
$E(L_{1c})$	0.72	1.70	1.81	1.81
$E(X_{1c})$	1.18	1.90	1.98	1.98
$\Delta(\Gamma\text{-}L)$	0.56	0.29	0.29	0.29
$\Delta(\Gamma\text{-}X)$	1.02	0.49	0.46	0.46
$m_e^*(\Gamma_{1c})$	0.01	0.066	0.064	0.067
$m_t^*(L_{1c})$	0.10	0.10	0.077	0.075
$m_l^*(L_{1c})$	1.73	1.73	2.18	1.90
$m_t^*(X_{1c})$	0.21	0.18	0.20	0.23
$m_l^*(X_{1c})$	1.06	1.88	1.30	1.30

[a]Refs. 14 and 15.
[b]Ref. 16.
[c]Ref. 13.

Each electronic state $\psi_i(\mathbf{r})$ of the nanosystem can be expanded in a complete set of bulk Bloch states $u_{n,\mathbf{k}}(\mathbf{r})e^{i\mathbf{k}\cdot\mathbf{r}}$.[19] If we sum over the bands n at a given first Brillouin zone wave vector $\mathbf{k}$, we obtain the "majority representation" decomposition of the quantum-dot state i (Ref. 20) as

$$P_i(\mathbf{k}) = \sum_{n=1}^{N_{\text{bands}}} |\langle \psi_i(\mathbf{r})|u_{n,\mathbf{k}}(\mathbf{r})e^{i\mathbf{k}\cdot\mathbf{r}}\rangle|^2. \quad (1)$$

To determine the reciprocal-space character of the state i, we introduce the weight functions w_i^Γ, w_i^L, and w_i^X, which are calculated by summing $P_i(\mathbf{k})$ over the $\mathbf{k}$ points contained in a spherical region around Γ, *L*, and *X*, respectively, as follows:

$$w_i^{\Gamma(X,L)} = 100 \sum_{\mathbf{k}\in\Omega_{\Gamma(X,L)}} P_i(\mathbf{k}). \quad (2)$$

The spheres Ω_Γ, Ω_L, and Ω_X in the fcc Brillouin zone have the same radius. The number of $\mathbf{k}$ points in Eq. (2) depends on the supercell size. For $R=1.59$ nm, there is a total of 733 $\mathbf{k}$ points in the sphere centered at the Γ point, 2049 $\mathbf{k}$ points in the spheres centered at the six *X* points, and 2348 $\mathbf{k}$ points in the spheres centered at the eight *L* points.

III. DIRECT-TO-INDIRECT TRANSITION IN FREESTANDING GaAs QUANTUM DOTS

A. Simple effective-mass estimate

The simplest approach to evaluate type-(i) electronic transitions is to assume that the size dependence of the individual electronic levels in a dot is given by the *single-band*

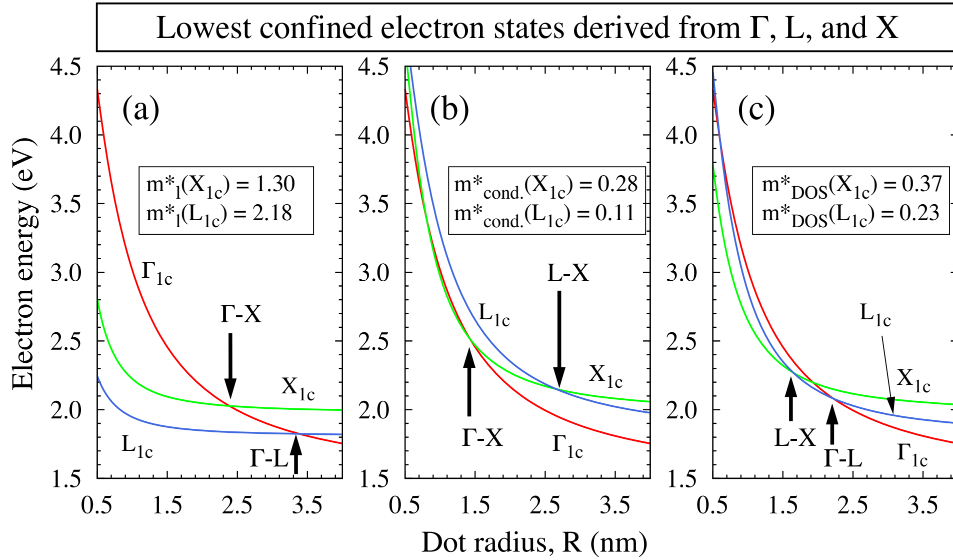

FIG. 2. (Color online) Direct-to-indirect crossover (vertical arrows) in spherical GaAs dots as obtained from the single-band effective mass model, with different choices of X-valley and L-valley effective masses (given in the inset of each panel). The band offsets $\Delta E_c(\Gamma-\Gamma)=3.33$ eV, $\Delta E_c(X-X)=3.03$ eV, and $\Delta E_c(L-L)=3.36$ eV, and the Γ electron effective mass $m^*_{\mathrm{cond}}(\Gamma_{1c})=m^*_{\mathrm{DOS}}(\Gamma_{1c})=0.064m_0$ are taken from pseudopotential calculations (Table I). The X and L valley effective masses are defined in three ways by (a) the heaviest masses (i.e., m^*_l in the longitudinal direction), (b) the reciprocal weighted average mass, and (c) the averaged density of state mass. Different effective masses give different crossover radii.

effective mass approximation. One can then calculate the critical radius R_c at which two levels α and β cross. In the single-band EMA the coupling matrix element $V_{\alpha,\beta}$ is assumed to vanish, so the levels α and β may only *cross* (as opposed to *anticross*) as a function of size. The single-band EMA approach raises the question of which effective mass should be used to describe $\varepsilon_\alpha(R)$ when α has an anisotropic effective mass, as in the case of the X and L valleys in the fcc Brillouin zone. There are three popular definitions of "effective mass" for a valley with longitudinal mass m_l and transversal mass m_t: (a) use the largest component of a given valley, (b) use the reciprocal weighted average $m^*_{\mathrm{cond}}=3/(1/m_l+2/m_t)$, and (c) use the density of state mass $m^*_{\mathrm{DOS}}=\sqrt[3]{m_l m_t^2}$. Figure 2(a) shows that if one uses the largest mass $m^*_l(X_{1c})=1.30$ and $m^*_l(L_{1c})=2.18$ then one finds a Γ-L crossing at $R=3.4$ nm and a Γ-X crossing at $R=2.4$ nm. In contrast, Fig. 2(b) shows that if one uses the reciprocal weighted average mass, i.e., $m^*_{\mathrm{cond}}(X_{1c})=0.28$ and $m^*_{\mathrm{cond}}(L_{1c})=0.11$, one finds a L-X crossing at $R=2.7$ nm and a Γ-X crossing at $R=1.4$ nm. Finally, Fig. 2(c) shows that if one adopts the DOS mass $m^*_{\mathrm{DOS}}(X_{1c})=0.37$ and $m^*_{\mathrm{DOS}}(L_{1c})=0.23$ one finds a Γ-L crossing at $R=2.2$ nm and a L-X crossing at $R=1.7$ nm. Naturally, in this particle-in-a-box approach, the dependence of ε_α on R is R^{-2}—a much stronger dependence than expected from realistic calculations,[21] where more than one bulk band can participate in forming the dot wave functions. We will next examine the crossing obtained with a multiband (pseudopotential) description, finding that none of the simple effective mass predictions holds.

B. A multiband pseudopotential approach

Figure 3(a) shows the pseudopotential calculated three

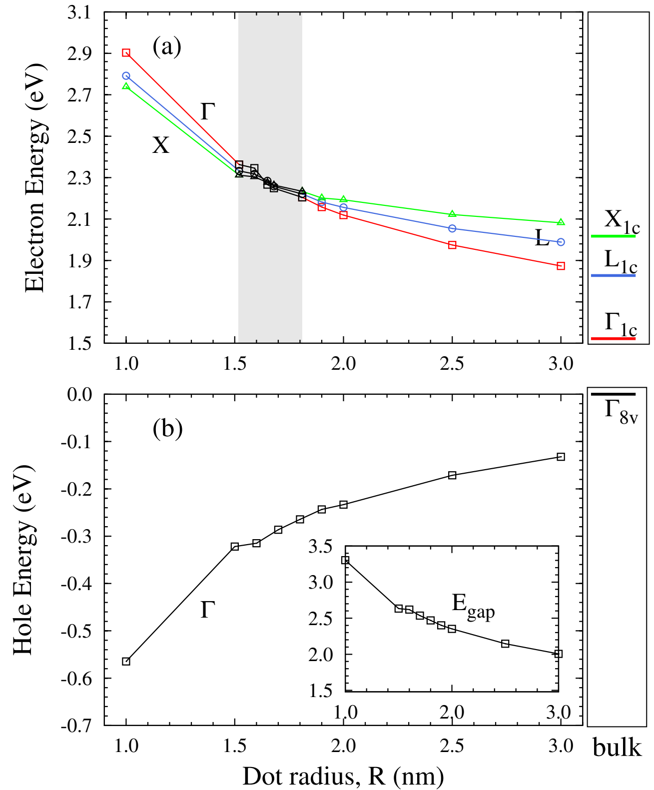

FIG. 3. (Color online) Electron and hole energies of freestanding spherical GaAs dots. (a) Lowest confined electron states derived from Γ, L, and X, respectively [identified in terms of bulk character via the majority representation Eq. (1)]. The shaded area indicates the Γ-X transition region, which is described in more detail in Fig. 4. (b) Highest hole level $\varepsilon(h_0)$. The inset in (b) gives the band gap energy as a function of dot radius.

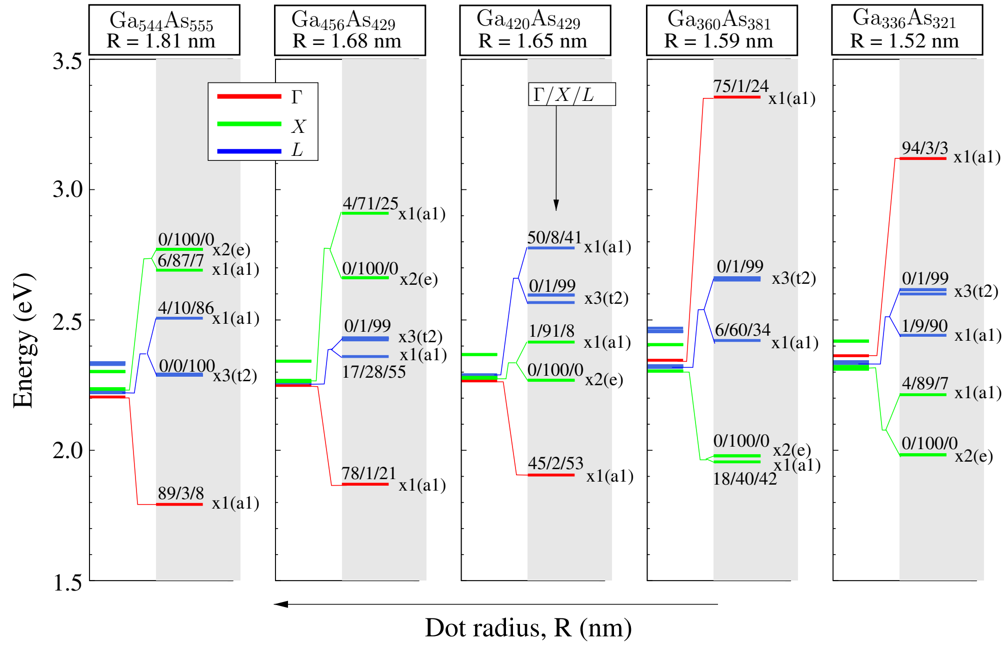

FIG. 4. (Color online) Analysis of the lowest-energy confined electron states of spherical GaAs dots in terms of the percent $w_\Gamma/w_X/w_L$ of Γ, X, and L character according to the majority representation decomposition of Eq. (1). The left-hand side of each panel gives the energy levels ε_i, whereas the gray-shaded right-hand size gives the wave function symmetry and degeneracy.

lowest-energy confined electron states, with a_1 symmetry, of freestanding spherical GaAs dots as a function of dot size. The identity of these states in terms of bulk character is determined from their majority representation [Eq. (1)][20] and is indicated in Fig. 3. The CBM character changes from Γ-like to X-like as the size is reduced. However, near the transition point, the levels are closely spaced and difficult to discern. Thus, in Fig. 4, we provide, on an expanded scale, a set of panels each giving, for a specific dot size, the conduction-band states in order of increasing energy $(e_0, e_1, e_2, \ldots)$ and, for each state, the decomposition of its wave function into Γ-like, X-like, and L-like components (using the notation $w_\Gamma/w_X/w_L$). In Fig. 5, we show the majority representation of the CBM wave functions of different GaAs dots in the fcc Brillouin zone. We see that for large dots, the lowest electron level e_0 is primarily Γ-like, transforming at R=1.81 nm to $\Gamma/X/L$ percentages of 89/3/8, at R=1.68 nm to 78/1/21, and at R=1.65 nm to 42/2/53. At a slightly smaller radius of R=1.59 nm, we find that e_0 becomes 18/40/42, and at R=1.52 nm it is a pure X-like state 0/100/0.

We conclude that the electronic transition is Γ to X, not Γ to L as suggested by tight-binding calculations.[8] We find that the nature of the transition depends both on the rate of increase of individual energy levels $\varepsilon_\alpha(R)$ as the radius R decreases (Fig. 3), and on the wave functions of the system. It would appear that some of the standard electronic structure methods may not accurately capture both aspects. Indeed, density-functional theory in the local-density approximation fails to describe effective masses (Table I) and wave function coupling,[14,15] while tight-binding calculations[8,16] may have various degrees of success in properly depicting the wave functions.

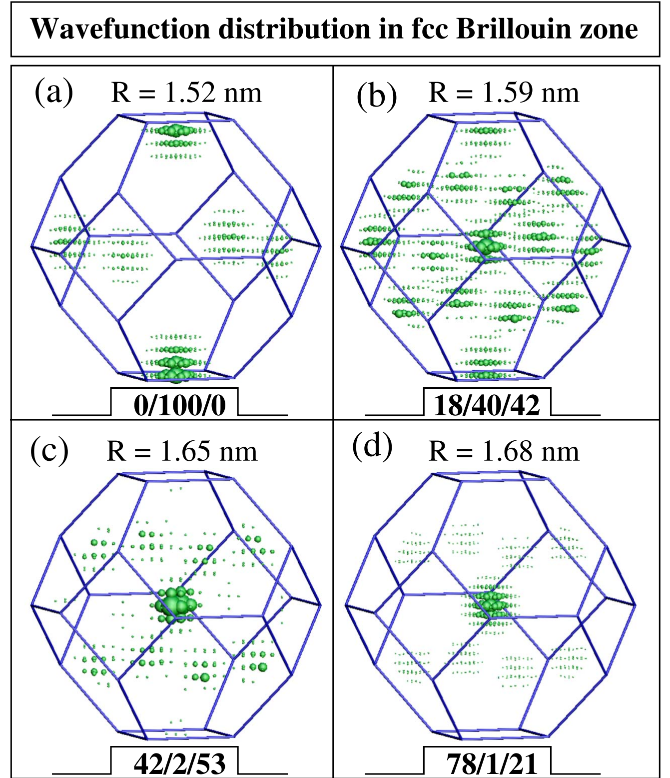

FIG. 5. (Color online) The majority-representation decomposition [Eq. (1)] showing regions in the fcc Brillouin zone from which the lowest-energy dot wave function derives. Results are given for four GaAs dots of radius R=1.52, 1.59, 1.65, and 1.68 nm. The percent wave function weights $w_\Gamma/w_X/w_L$ are also given in the figure.

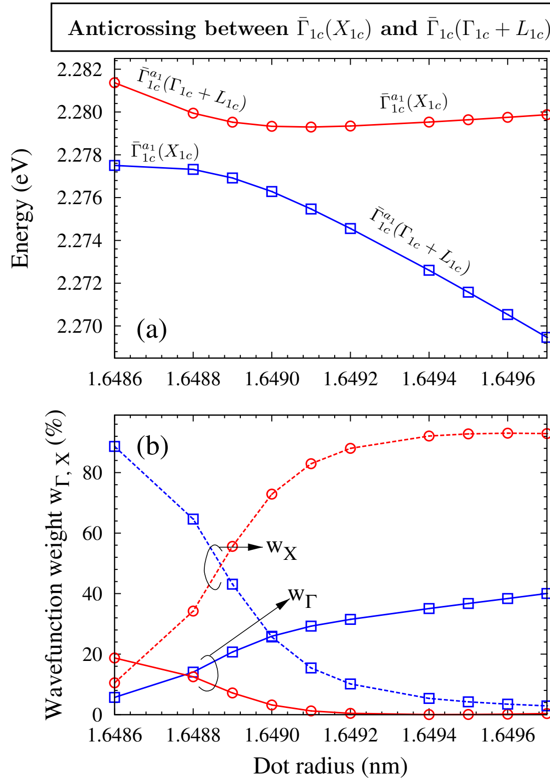

FIG. 6. (Color online) (a) Dependence of the two lowest-energy electron levels of a $R=1.65$ nm freestanding GaAs dot on pressure, as determined by slowly changing the lattice constant, and therefore the dot radius. (b) Percent wave function weights w_Γ and w_X of the two states shown in (a).

C. Pressure-induced direct-to-indirect transition

When pressure is applied to a direct-gap GaAs dot, a Γ-X transition of the CBM takes place, which is driven by the different deformation potentials of Γ-derived and X-derived states.[22] Since the Γ_{1c}-derived states of a quantum dot with the T_d point group symmetry belong to the a_1 representation, the Γ-X transition will be an *anticrossing* transition if the lowest-energy X-derived state has the a_1 symmetry, while it will be a *crossing* transition if the lowest-energy X-derived state belongs to a different representation. We find that the lowest-energy X-derived conduction-band state has the a_1 symmetry,[23] so we expect the Γ-X pressure-induced transition to be an anticrossing transition. Figure 6 shows the calculated energy levels of a $R=1.65$ nm GaAs quantum dot, when we gently and continuously change the volume of the dot. This is accomplished by reducing the radius R of the quantum dot according to $R(x)=(x\cdot a_0)(R_0/a_0)$, where $R_0=1.65$ nm, $a_0=5.65$ Å is the zero-pressure lattice constant, and the variable x (with $x=0.999-1.0$) changes the lattice constant. Figure 6 clearly shows an anticrossing transition between Γ and X with $2V_{\Gamma X}\sim 2$ meV.

IV. DIRECT-TO-INDIRECT TRANSITION IN GaAs/AlGaAs QUANTUM DOTS

The CBM of the $Al_xGa_{1-x}As$ random alloy changes from Γ_{1c} to X_{1c} as the Al concentration x increases above $x_c \simeq 0.4$.[13] Figure 7 shows the energies of the Γ_{15v}, Γ_{1c}, X_{1c}, and L_{1c} electronic levels of the $Al_xGa_{1-x}As$ alloy as a function of the Al concentration x. At low Al concentrations ($x<x_c$) the VBM has the Γ_{15v} symmetry, and the CBM has the Γ_{1c} symmetry, so the band gap is direct. At larger Al concentrations ($x>x_c$) the CBM has the X_{1c} symmetry, so the band gap is indirect. When a GaAs quantum dot is embedded in an $Al_xGa_{1-x}As$ alloy, its energy levels depend on the dot radius R as well as the alloy Al concentration x. For $x<x_c$ and $R>R_c(x)$ [where $R_c(x)$ is a critical radius that depends on the Al concentration[10]] both the VBM and the CBM are localized on the quantum dot and originate from the Γ point, so the band gap is direct both in real space and in reciprocal space. However, as pointed out in Ref. 10, if the dot radius is smaller than $R_c(x)$, the CBM becomes delocalized over the entire dot+matrix system, and the oscillator strength of the VBM-CBM transition decreases. For $x>x_c$, the CBM of the alloy is X-like. If $R>R_c(x)$, the CBM of the dot+alloy system is localized in the dot and the band gap is direct both in reciprocal space and in real space. If $R<R_c(x)$, the CBM of the quantum dot is above the CBM of the alloy, so the band gap becomes indirect both in real space and in reciprocal space.[10]

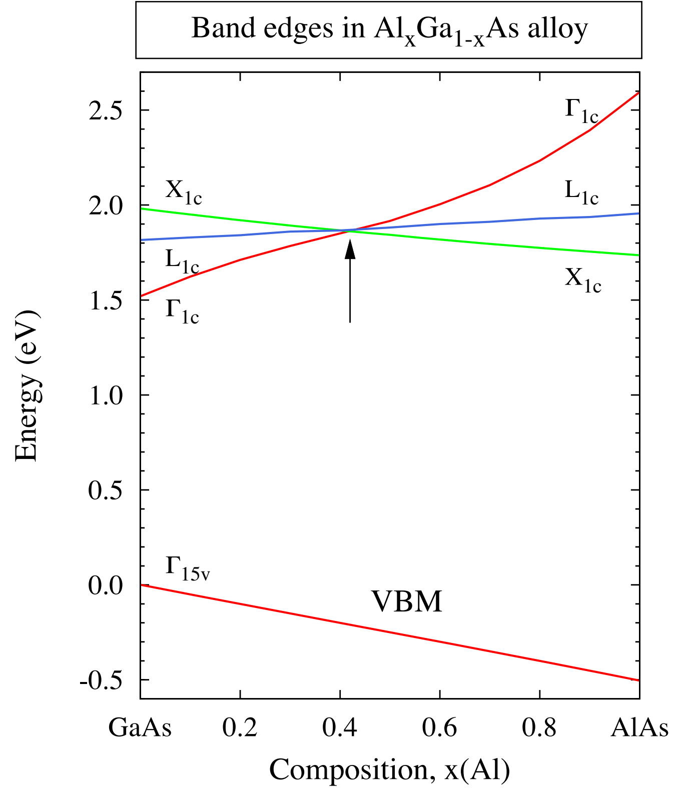

FIG. 7. (Color online) The composition-dependent band-edge energies of $Al_xGa_{1-x}As$. The vertical arrow indicates the direct-to-indirect crossover of the conduction band.

In Ref. 10, we used the single-band effective-mass approximation to calculate the electronic phase diagram of spherical GaAs quantum dots embedded in $Al_xGa_{1-x}As$. A similar calculation using the empirical pseudopotential method would be prohibitively expensive, so in the following, we will consider two limiting cases: (i) A spherical

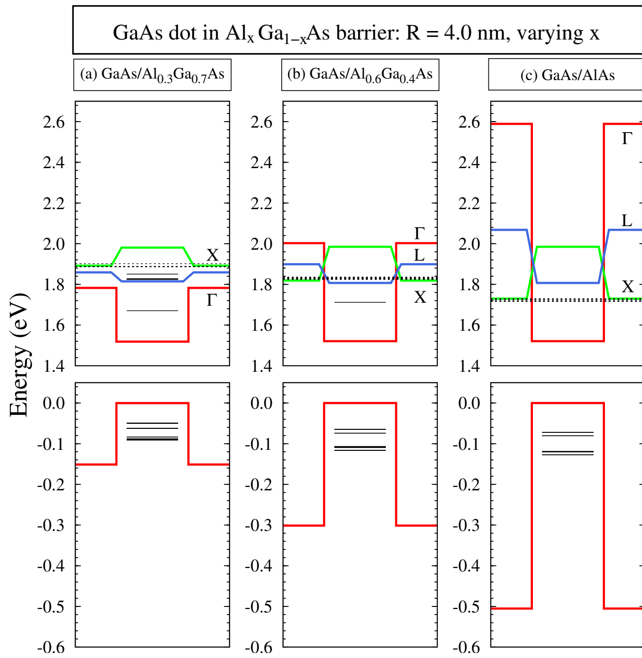

FIG. 8. (Color online) Confined energy levels (thin black lines) of (a) GaAs/$Al_{0.3}Ga_{0.7}As$, (b) GaAs/$Al_{0.6}Ga_{0.4}As$, and (c) GaAs/AlAs quantum dots of radius R=4.0 nm. We show three types of confining barriers, Γ-barrier in red, X-barrier in green, and L-barrier in blue. The dashed black lines indicate eigenstates located in the barrier and derived from bulk X Bloch states.

GaAs dot of radius R=4.0 nm embedded in an $Al_xGa_{1-x}As$ alloy of varying Al concentration (x=0.3, 0.6, and 1.0, see Fig. 8), and (ii) a spherical GaAs dot of variable radius R (with $4<R<5$ nm) embedded in pure AlAs (Fig. 9). The results are as follows:

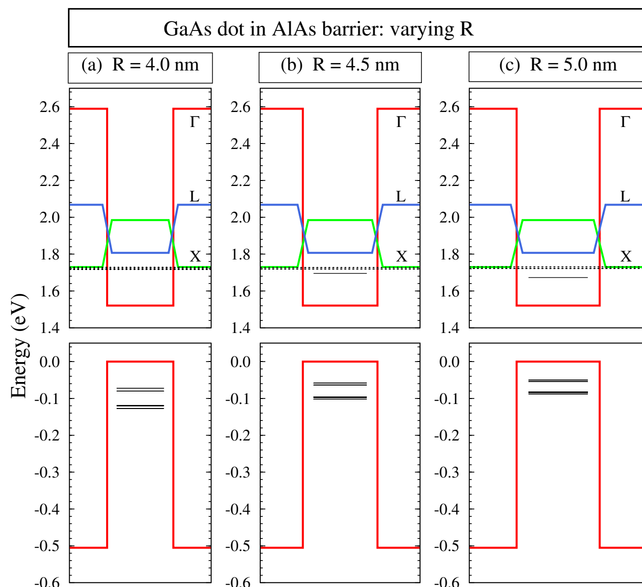

FIG. 9. (Color online) Confined energy levels (thin black lines) of GaAs/AlAs dots of radius R=4.0, 4.5, and 5.0 nm. We show three types of confining barriers, Γ-barrier in red, X-barrier in green, and L-barrier in blue. The dashed black lines indicate eigenstates located in the barrier and derived from bulk X Bloch states.

(i) We find that the VBM and the CBM wave functions of a R=4.0 nm GaAs dot embedded in $Al_{0.3}Ga_{0.7}As$ [Fig. 8(a)] are located on the GaAs quantum dot and derive from the Γ point (Fig. 10). The band gap is direct both in real space and reciprocal space. As the Al concentration in the matrix increases [Figs. 8(b) and 8(c)], the potential barrier experienced by the Γ-derived CBM of the quantum dot increases, because the Γ_{1c} level of the alloy moves up in energy. At the same time, the X_{1c} level of the alloy moves down in energy, because the Al concentration increases. We find that the band gap of the GaAs/$Al_{0.6}Ga_{0.4}As$ system is still direct [Fig. 8(b)], but the band gap of the GaAs/AlAs system is indirect both in real space and in reciprocal space [Fig. 8(c)]. The CBM wave functions of the R=4.0 nm GaAs dot for different Al concentrations of the alloy (x=0.3, 0.6, and 1.0) clearly demonstrate the direct/indirect transition in real space (Fig. 10).

(ii) As the size of a GaAs dot embedded in pure AlAs increases from 4.0 to 5.0 nm (Fig. 9), the quantum confinement decreases, whereas the electronic levels of the alloy remain the same. As a result, the CBM changes its real-space localization from the alloy back to the quantum dot (see Figs. 9 and 10), and its reciprocal-space character from X-like to Γ-like. Figure 10 depicts the CBM wave functions of GaAs dots of radius R=4.0 and 4.5 nm embedded in AlAs, clearly showing the real-space electronic transition.

V. EXPERIMENTAL SITUATION FOR TESTING OUR PREDICTIONS

Our prediction of a direct-to-indirect transition for freestanding GaAs spherical nanocrystals of radius $R\sim1.6$ nm calls for experimental investigation. It appears, however, that good quality (well-passivated) freestanding GaAs nanocrystals are difficult to make. Indeed, colloidal synthesis that was very successful for CdSe (e.g., Ref. 3) has hardly been successful for GaAs. The first colloidal GaAs nanocrystals were fabricated by Olshavsky *et al.*[24] Nozik and his colleagues[25–27] systematically measured the optical spectrum of colloidal GaAs nanocrystals. After separating the nanocrystals by a series of ultrafiltrations with pore size of 700, 100, and 15 Å, they found that there was no absorption peak for the 15 Å filtrate while there was a clear peak for 700 and 100 Å filtrates. This can be due to the low concentration of nanocrystals in this colloid or to the transition becoming indirect. Malik *et al.*[28] recently fabricated GaAs nanocrystals from $GaCl_3$ and $As(NMe_2)_3$ in 4-ethylpydidine[28] with TEM measured size from 1 to 3 nm in radius. For small GaAs nanocrystals, they observed two absorption peaks that we tentatively assign to the partially allowed Γ-to-X transitions (see Fig. 4 here for R=1.59 nm and R=1.65 nm), followed by the Γ-to-Γ transition. Another commonly used method for fabricating spherical GaAs dots is by ion implantation of Ga^+ and As^- into SiO_2 matrix followed by thermal annealing.[29,30] Such GaAs dots are characterized by an average radius of $\sim$3 nm and a broad photoluminescence peak centered at 1.6–1.8 eV. Recently, the

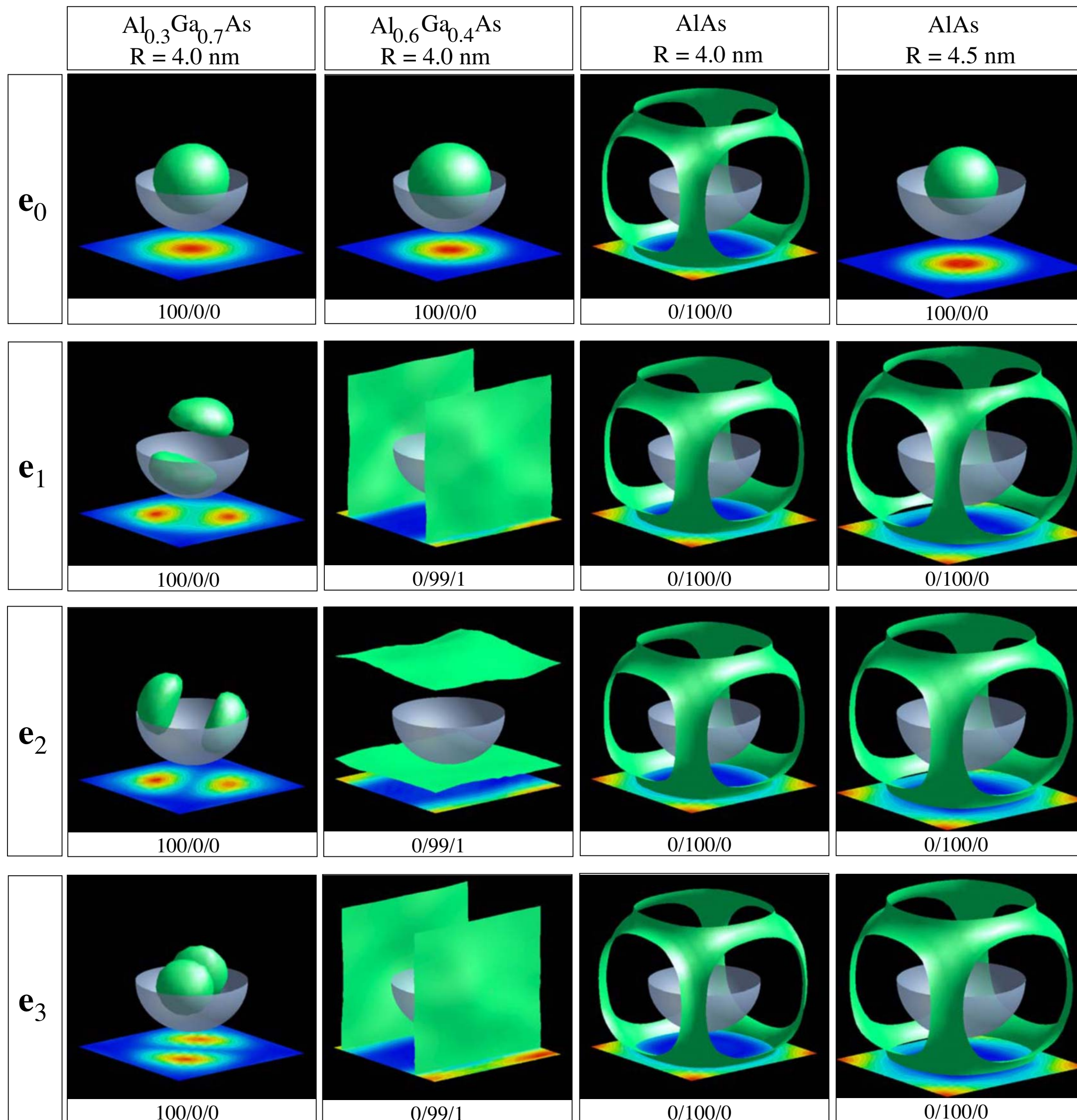

FIG. 10. (Color online) Real-space wave function isosurfaces of the four lowest-energy electron states of $GaAs/Al_{0.3}Ga_{0.7}As$ ($R=4.0$ nm), $GaAs/Al_{0.6}Ga_{0.4}As$ ($R=4.0$ nm), and GaAs/AlAs ($R=4.0$ nm and $R=4.5$ nm) quantum dots. The numbers at the bottom of each panel give the majority-representation decomposition $w_\Gamma/w_X/w_L$ [Eq. (2)]. The wave function isosurfaces are shown in green, whereas the dot itself is shown as a transparent white sphere. Each panel also shows the 2D wave function contour plot (at bottom).

pulsed laser ablation method was used to synthesize spherical GaAs nanocrystals with size of 5–8 nm in diameter and emission at 2.389 eV with a shoulder at 2.254 eV.[31]

The direct-to-indirect transition in $Al_xGa_{1-x}As$ embedded GaAs dot depends on both the Al concentration in the matrix and the dot size (Figs. 7 and 8). $Al_{0.3}Ga_{0.7}As$-embedded self-assembled GaAs quantum dots were first grown by modified droplet epitaxy by Koguchi *et al.*[32] The photoluminescence peaks of pyramidal-shaped GaAs quantum dots with base size of 10×15 nm^2 and 16×20 nm^2 are at 1.78 and 1.65 eV, respectively.[33] These dots undergo a direct-to-indirect transition at a pressure of 18.3 kbar.[34] Rastelli *et al.*[35] produced inverted lens-shaped $GaAs/Al_xGa_{1-x}As$ ($x=0.35-0.45$) dots via hierarchical self-assembly by combining Stranski–Krastanov growth and *in situ* etching. The dots luminesce at 1.6–1.7 eV.[35] Zhu *et al.*[36] made a novel $GaAs/Al_xGa_{1-x}As$ ($x=0.12-0.37$) quantum wire/dot system with a photoluminescence peak at 1.57–1.63 eV. Our prediction of direct-to-indirect transition in $Al_xGa_{1-x}As$ embedded GaAs dot is awaiting experimental testing.

VI. CONCLUSIONS

By using atomistic pseudopotential calculations, we have studied direct/indirect electronic transitions in freestanding and AlGaAs-embedded spherical GaAs quantum dots. We find that freestanding GaAs dots undergo a reciprocal-space (type i) direct-to-indirect transition when their radius decreases below 1.65 nm. The lowest conduction-band state changes its character from Γ-like to X-like, in agreement with Ref. 9, but not with Ref. 8, which predicted an L-derived CBM at small dot sizes. In the case of GaAs quantum dots embedded in $Al_xGa_{1-x}As$, we find that the CBM

undergoes a simultaneous reciprocal-space (type i) and real-space (type ii) direct/indirect transition when the radius of the dot becomes smaller than a critical value R_c that depends on the alloy composition. For example, the CBM of a $R=4.0$ nm GaAs dot embedded in AlAs is localized in the AlAs matrix, and derives from the X_{1c} states of the alloy. The CBM becomes dot-localized and Γ-derived when the size of the dot increases above 5.0 nm, or alternatively when the Al concentration in the matrix decreases below $x=0.6$. Our results determine the conditions that must be satisfied to achieve a direct band gap, and thus strong photoluminescence, in GaAs nanostructures.

ACKNOWLEDGMENTS

J.-W.L. would like to thank S.H. Wei for helpful discussion on the symmetry of zinc blende electronic states. This work was funded by the U.S. Department of Energy, Office of Science, Basic Energy Science, Materials Sciences and Engineering, under Contract No. DE-AC36-99GO10337 to NREL.

*Corresponding author: alex_zunger@nrel.gov

[1] R. Turton, *The Quantum Dot* (Oxford University, New York, 1996).

[2] L. Bányai and S. W. Koch, *Semiconductor Quantum Dots* (World Scientific, Singapore, 1993).

[3] V. I. Klimov, A. A. Mikhailovsky, S. Xu, A. Malko, J. A. Hollingsworth, C. A. Leatherdale, H. J. Eisler, and M. G. Bawendi, Science **290**, 314 (2000).

[4] V. I. Klimov, S. A. Ivanov, J. Nanda, M. Achermann, I. Bezel, J. A. McGuire, and A. Piryatinski, Nature (London) **447**, 441 (2007).

[5] R. Schmidt, U. Scholz, M. Vitzethum, R. Fix, C. Metzner, P. Kailuweit, D. Reuter, A. Wieck, M. C. Hübner, S. Stufler, A. Zrenner, S. Malzer, and G. H. Döhler, Appl. Phys. Lett. **88**, 121115 (2006).

[6] M. Bruchez, Jr., M. Moronne, P. Gin, S. Weiss, and A. P. Alivisatos, Science **281**, 2013 (1998).

[7] A. J. Williamson, A. Franceschetti, H. Fu, L. W. Wang, and A. Zunger, J. Electron. Mater. **28**, 414 (1999).

[8] J. G. Díaz and G. W. Bryant, Phys. Rev. B **73**, 075329 (2006).

[9] A. Franceschetti and A. Zunger, J. Chem. Phys. **104**, 5572 (1996).

[10] A. Franceschetti and A. Zunger, Phys. Rev. B **52**, 14664 (1995).

[11] L. W. Wang, A. Franceschetti, and A. Zunger, Phys. Rev. Lett. **78**, 2819 (1997).

[12] L. W. Wang and A. Zunger, Phys. Rev. B **51**, 17398 (1995).

[13] I. Vurgaftman, J. R. Meyer, and L. R. Ram-Mohan, J. Appl. Phys. **89**, 5815 (2001).

[14] C. Persson and S. Mirbt, Braz. J. Phys. **36**, 286 (2006).

[15] C. Persson and A. Zunger (unpublished).

[16] T. B. Boykin, G. Klimeck, R. C. Bowen, and F. Oyafuso, Phys. Rev. B **66**, 125207 (2002).

[17] We define the effective radius $R=a_0/2\sqrt[3]{3N/4\pi}$, where a_0 is lattice constant of GaAs and N is number of atoms.

[18] L. W. Wang and A. Zunger, J. Chem. Phys. **100**, 2394 (1994).

[19] L. W. Wang and A. Zunger, Phys. Rev. B **59**, 15806 (1999).

[20] L. W. Wang, L. Bellaiche, S. H. Wei, and A. Zunger, Phys. Rev. Lett. **80**, 4725 (1998).

[21] J. W. Luo, S. S. Li, J. B. Xia, and L. W. Wang, Appl. Phys. Lett. **88**, 143108 (2006).

[22] U. Venkateswaran, M. Chandrasekhar, H. R. Chandrasekhar, T. Wolfram, R. Fischer, W. T. Masselink, and H. Morkoç, Phys. Rev. B **31**, 4106 (1985).

[23] In a quantum dot with the T_d point-group symmetry, states derived from the L point have t_2 or a_1 symmetry, while states derived from the X point have a_1 or e symmetry. Thus, it is possible to identify states with the a_1 symmetry based on the fact that a_1 is the only nondegenerate representation.

[24] M. A. Olshavsky, A. N. Goldstein, and A. P. Alivisatos, J. Am. Chem. Soc. **112**, 9438 (1990).

[25] H. Uchida, C. J. Curtis, and A. J. Nozik, J. Phys. Chem. **95**, 5382 (1991).

[26] H. Uchida, C. J. Curtis, P. V. Kamat, K. M. Jones, and A. J. Nozik, J. Phys. Chem. **96**, 1156 (1992).

[27] O. I. Mićić and A. J. Nozik, J. Lumin. **70**, 95 (1996).

[28] M. A. Malik, P. O'Brien, S. Norager, and J. Smith, J. Mater. Chem. **13**, 2591 (2003).

[29] Y. Kanemitsu, H. Tanaka, S. Mimura, and T. Kushida, J. Lumin. **83-84**, 301 (1999).

[30] Y. Kanemitsu, H. Tanaka, Y. Fukunishi, T. Kushida, K. S. Min, and H. A. Atwater, Phys. Rev. B **62**, 5100 (2000).

[31] J. Perriére, E. Millon, M. Chamarro, M. Morcrette, and C. Andreazza, Appl. Phys. Lett. **78**, 2949 (2001).

[32] N. Koguchi and K. Ishige, Jpn. J. Appl. Phys., Part 1 **32**, 2052 (1993).

[33] K. Watanabe, S. Tsukamoto, Y. Gotoh, and N. Koguchi, J. Cryst. Growth **227-228**, 1073 (2001).

[34] M. Yamagiwa, N. Sumita, F. Minami, and N. Koguchi, J. Lumin. **108**, 379 (2004).

[35] A. Rastelli, S. Stufler, A. Schliwa, R. Songmuang, C. Manzano, G. Costantini, K. Kern, A. Zrenner, D. Bimberg, and O. G. Schmidt, Phys. Rev. Lett. **92**, 166104 (2004).

[36] Q. Zhu, K. F. Karlsson, E. Pelucchi, and E. Kapon, Nano Lett. **7**, 2227 (2007).